

Understanding of impact of carbon doping on background carrier conduction in GaN

Zhenxing Liu(刘振兴), Liuan Li(李柳暗), Jinwei Zhang(张津玮), Qianshu Wu(吴千树), Yapeng Wang(王亚朋), Qiuling Qiu(丘秋凌), Zhisheng Wu(吴志盛), and Yang Liu(刘扬)

Citation: Chin. Phys. B, 2021, 30 (**10**): 107201. DOI: 10.1088/1674-1056/abfa0d
Journal homepage: http://cpb.iphy.ac.cn; http://iopscience.iop.org/cpb

What follows is a list of articles you may be interested in

Fang-Howard wave function modelling of electron mobility in AlInGaN/AlN/InGaN/GaN double heterostructures

Yao Li(李姚) and Hong-Bin Pu(蒲红斌)
Chin. Phys. B, 2021, 30 (**9**): 097201. DOI: 10.1088/1674-1056/abea87

Temperature dependence on the electrical and physical performance of InAs/AlSb heterojunction and high electron mobility transistors

Jing Zhang(张静), Hongliang Lv(吕红亮), Haiqiao Ni(倪海桥), Zhichuan Niu(牛智川), Yuming Zhang(张玉明)
Chin. Phys. B, 2018, 27 (**9**): 097201. DOI: 10.1088/1674-1056/27/9/097201

Room-temperature terahertz detection based on CVD graphene transistor

Yang Xin-Xin, Sun Jian-Dong, Qin Hua, Lv Li, Su Li-Na, Yan Bo, Li Xin-Xing, Zhang Zhi-Peng, Fang Jing-Yue
Chin. Phys. B, 2015, 24 (**4**): 047206. DOI: 10.1088/1674-1056/24/4/047206

An improved EEHEMT model for kink effect on AlGaN/GaN HEMT

Cao Meng-Yi, Lu Yang, Wei Jia-Xing, Chen Yong-He, Li Wei-Jun, Zheng Jia-Xin, Ma Xiao-Hua, Hao Yue
Chin. Phys. B, 2014, 23 (**8**): 087201. DOI: 10.1088/1674-1056/23/8/087201

Electron mobility in the linear region of AlGaN/AlN/GaN heterostructure field-effect transistor

Yu Ying-Xia, Lin Zhao-Jun, Luan Chong-Biao, Wang Yu-Tang, Chen Hong, Wang Zhan-Guo
Chin. Phys. B, 2013, 22 (**6**): 067203. DOI: 10.1088/1674-1056/22/6/067203

Understanding of impact of carbon doping on background carrier conduction in GaN*

Zhenxing Liu(刘振兴)[1], Liuan Li(李柳暗)[1], Jinwei Zhang(张津玮)[1], Qianshu Wu(吴千树)[1], Yapeng Wang(王亚朋)[1], Qiuling Qiu(丘秋凌)[1], Zhisheng Wu(吴志盛)[1], and Yang Liu(刘扬)[1,2,†]

[1] *School of Electronics and Information Technology, Sun Yat-Sen University, Guangzhou* 510275, *China*
[2] *State Key Laboratory of Optoelectronic Materials and Technologies, Sun Yat-sen University, Guangzhou* 510275, *China*

(Received 4 January 2021; revised manuscript received 15 April 2021; accepted manuscript online 21 April 2021)

The impact of carbon doping on the background carrier conduction in GaN has been investigated. It is found that the incorporation of carbon can effectively suppress the n-type background carrier concentration as expected. Moreover, from the fitting of the temperature-dependent carrier concentration and mobility, it is observed that high nitrogen–vacancy (V_N) dominates the background carrier at room temperature which consequently results in n-type conduction. The doping agent (carbon atom) occupies the nitrogen site of GaN and forms C_N deep acceptor as revealed from photoluminescence. Besides, a relatively low hole concentration is ionized at room temperature which was insufficient for the compensation of n-type background carriers. Therefore, we concluded that this background carrier concentration can be suppressed by carbon doping, which substitutes the N site of GaN and finally decreases the V_N.

Keywords: electrical properties and parameters, semiconductor materials, chemical vapor deposition, electronic transport

PACS: 72.20.−i, 72.80.Ey, 72.10.Bg, 72.10.−d **DOI:** 10.1088/1674-1056/abfa0d

1. Introduction

GaN-based devices have promising applications in the field of power electronics due to their superior properties.[1,2] In order to realize the characteristics and minimize the vertical leakage current of high breakdown voltage, a semi-insulating or high resistivity GaN layer can easily prevent the undesired parallel current paths which are beneath the two-dimensional electron gas channel. However, it is already reported that the unintentionally doped-GaN exhibits n-type conductivity. These unintentional donor impurities are O,[3] Si,[4] and nitrogen–vacancy (V_N).[5,6] Earlier calculations[7] reveal that V_N may not be the major participants in the n-type GaN as its formation energy is very high in n-type materials. Recently, a group from the Helsinki University of Technology[5] demonstrated that nitrogen vacancies can be the major participants in the defect kinetics of n-type GaN. This V_N is mainly derived from the activation energy of self-diffusion in the nitrogen sublattice. Conventional synthetic techniques can easily produce V_N in the nitrogen sublattice of GaN. Conventional techniques such as thermal decomposition (metal–organic chemical vapor deposition) can occur above 900 °C, where the evaporated nitrogen from the sample surface improves the concentration of V_N.[5–9] However, the mechanism behind this is still unclear and the major participants in the n-type GaN are still under debate.

Generally, high resistivity of the materials can be achieved through two different techniques such as (i) eliminating the background impurities[10] and (ii) introducing the compensated acceptors. In previous reports, iron (Fe)[11,12] and carbon (C)[13–20] atoms are used as a compensator. Besides, the generation of intentionally edge dislocation in GaN[21,22] are also used as a compensator. Compared to Fe-doped GaN, the incorporation of C atom has produced a significantly high resistive layer. This is due to its wide doping range, better stability, and weak memory effect. The theoretical calculation shows that carbon atoms can preferably substitute the nitrogen site (C_N) and form a deep C_N acceptor in GaN, verified by many methods.[23–26] The PL spectrum of carbon-doped-GaN shows blue luminescence (BL) and yellow luminescence (YL) peaks at around 2.8 eV and 2.2 eV, along with the band edge (BE) luminescence at around 3.4 eV. The C_N acceptors with a negative-to-neutral charge state (−/0) (0.9 eV above valence band) and a 0/+ level (0.4 eV above valence band)[25,26] are theoretically calculated which interpret the YL and BL luminescence, respectively. It is also recognized that these deep energy levels are difficult to be electrically ionized[27–31] and the compensation of background carrier is associated with the Fermi level pinning effect at around C_N acceptor energy level.[28–31] While the pinning effect occurs when the acceptor trap density is much higher than that of donor trap density, the fermi energy levels and background carrier concentration remain constant as C concentration increases. In this work

*Project partially supported by the National Key Research and Development Program of China (Grant No. 2017YFB0402800), the Key Research and Development Program of Guangdong Province, China (Grant No. 2020B010174003), the National Natural Science Foundation of China (Grant No. U1601210), and the Natural Science Foundation of Guangdong Province, China (Grant No. 2015A030312011).

†Corresponding author. E-mail: liuy69@mail.sysu.edu.cn

© 2021 Chinese Physical Society and IOP Publishing Ltd

the background concentration generally varies with the carbon doping concentration. The Fermi level pinning effect at around C_N acceptor can be excluded for the reduction of background carrier concentration. Therefore, the formation mechanism of high resistivity layer by C-doping is still under debate.

In this work, we have investigated the relationship between background carrier conduction and carbon doping in GaN on the sapphire substrate. On fitting the temperature-dependent carrier concentration and mobility, it is found that the background conduction at room temperature is dominated by the nitrogen–vacancy (V_N). The ionization concentration of C_N deep acceptor is lower, and the donor impurities cannot be sufficiently compensated. So, the incorporation of carbon atom has suppressed the background carrier in GaN, where C occupies the nitrogen site and reduces the V_N concentration.

2. Experimental

In order to focus on the impact of carbon doping on the background carrier conduction in GaN, we chose a quasi-vertical diode for C-doped material instead of high electron mobility transistor (HEMT) structure, as heterojunctions may cause unnecessary influence on the investigation of materials. Additionally, employing a quasi-vertical design results in a better field distribution and the peak electric field is moved away from the surface. The samples were prepared by metal–organic chemical vapor deposition using trimethylgallium (TMGa), trimethylaluminum (TMAl), and ammonia (NH_3) as the Ga, Al, and N precursors, respectively. Hydrogen was used as the carrier gas. From the bottom to top, the epitaxy structure consists of a 30-nm-thick low temperature (LT) GaN layer, a 500-nm-thick n^+-GaN layer (Si: $\sim 2\times10^{19}$ cm^{-3}), a 10-μm-thick carbon-doped GaN (C–GaN) bulk layer. All the epitaxy layers were grown at similar growth conditions except the top GaN bulk layer. Four samples (labeled as A, B, C, and D in Table 1) at different carbon concentrations were prepared by simply adjusting the pressure of the chamber. In our previous report, it has been described that the concentrations of carbon increase along with the decrease in reactor pressure.[14,15] This is also confirmed from the secondary ion mass spectrometry (SIMS) measurement (Fig. 1(c)). A quasi-vertical structure Schottky barrier diode (SBD) was fabricated for the electrical measurements (Fig. 1(a)). The process started with a 10-μm deep etching using inductively coupled plasma etching with a SiO_2 hard mask. After treatment of 5% tetra methyl ammonium hydroxide solution at 85 °C for 60 min, then a 200-nm thick SiO_2 passivation layer was deposited. A metal stack of Ti/Al/Ni/Au was evaporated and annealed at 870 °C for 30 s in a nitrogen ambient, to form a cathode electrode. Finally, Ni/Au (25 nm/65 nm) anode metal was evaporated. The Hall measurements were performed with the help of a common van der Pauw structure with four ohmic contact pads, prepared by annealing the indium (Fig. 1(b)). The three conductive layers are connected in shunt during measurement.

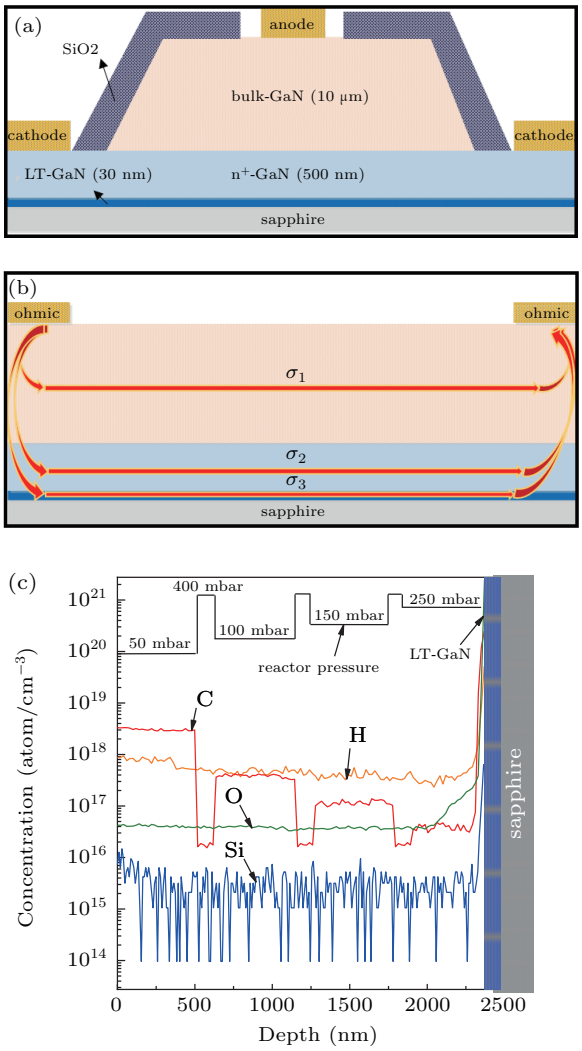


Fig. 1. (a) Schematic cross-section of the fabricated SBD on sapphire. (b) Multilayer conduction model for Hall measurement. σ_1, σ_2, and σ_3 are the 10-μm-thick carbon-doped GaN, the 500-nm-thick n^+-GaN layers, and the GaN/sapphire interface layer, respectively. (c) The secondary ion mass spectrometry (SIMS) measurement. The unit 1 bar = 10^5 Pa.

The carrier concentrations (the carrier is electron) are studied with the help of room-temperature Hall measurement which decreases along with the increase in the concentration of carbon doping (Fig. 2(a)). On the other hand, the crystallinity of GaN films is characterized by the full width at half maximum peaks of (002) and (102) planes changed slightly, with the screw- and edge-type dislocation density approximately around $\sim 10^7$ cm^{-2} and $\sim 10^8$ cm^{-2} levels, respectively. A 3 μm × 3μm scaled atomic force microscopy measurement shows that the root mean square roughness (RMS) of the as-grown samples are comparable. The specific on-resistance increases with C concentration extracted from the forward current–voltage (I–V) characteristics. The carrier spatial distribution extracted from capacitance–voltage (C–V) measurement (Fig. 2(b)) confirms the variation of carrier concentrations as summarized in Table 1.

Table 1. The growth parameters and electrical properties of GaN samples at different methods. Here, $\text{Hall}^{\text{mea.}}$ (RT) represents the carrier concentration, obtained from the room temperature (RT) Hall measurement and $\text{Hall}^{\text{extr.}}$ represents the carrier concentration which is extracted from the temperature-dependent Hall, using a bilayers conduction model. The deviation is defined as the ratio between the maximum and the minimum to the mean.

	Reactor pressure (mbar)	SIMS C (cm^{-3})	$\text{Hall}^{\text{mea.}}$ (RT) (cm^{-3})	N_D con. (cm^{-3}) (RT) Extracted from				V_N con. (cm^{-3}) Derived from fitting		Ionized C_N con. (cm^{-3})	
				$\text{Hall}^{\text{extr.}}$	*C–V* (net)	VRH	Deviation	*n*	*μ*	0.9 eV	0.4 eV
A	50	3.1×10^{18}	3.2×10^{16}	1.3×10^{16}	1.3×10^{16}	1.1×10^{16}	21.3%	9.1×10^{15}	1.1×10^{16}	8.3×10^{10}	4.9×10^{14}
B	100	4.3×10^{17}	1.5×10^{17}	2.9×10^{16}	2.7×10^{16}	2.8×10^{16}	9.5%	2.4×10^{16}	2.8×10^{16}	3.0×10^{10}	1.8×10^{14}
C	150	1.4×10^{17}	4.4×10^{17}	6.4×10^{16}	5.5×10^{16}	6.5×10^{16}	14.1%	5.6×10^{16}	6.2×10^{16}	1.5×10^{10}	–
D	250	3.3×10^{16}	3.7×10^{18}	1.4×10^{17}	1.3×10^{17}	1.4×10^{17}	2.1%	1.3×10^{17}	1.4×10^{17}	8.3×10^{9}	–

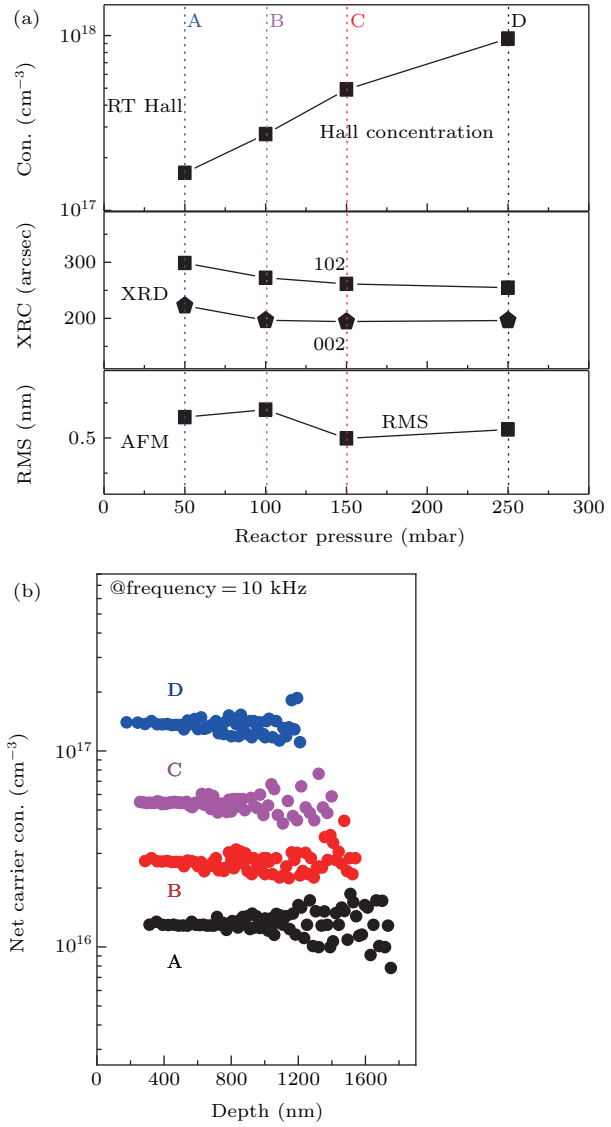


Fig. 2. Variation of carrier concentration (con.), dislocation density, and surface roughness *versus* reactor pressure. (b) The spatial distribution of net carrier concentration is calculated from the *C–V* curves of SBD. The unit 1 bar=10^5 Pa. RMS: mean square roughness, RT: room temperature, XRD: x-ray diffraction, AFM: atomic force microscopy.

It is worth noting that the carrier concentration of *C–V* is nearly one order of magnitude lower than that of Hall. However, they have a similar carrier decreasing trend as the concentration of carbon increases. This concentration discrepancy can be explained in terms of multilayer conduction in the following section.

3. Characteristics and discussion

The results of temperature-dependent Hall show that initially, the concentration of carrier (open circle in Fig. 3(a)) decreases along with the increase in temperature, and then it nearly shows no variation at relatively low temperature. This phenomenon is inconsistent with the classic donor frozen out and suggest another origination dominant high carrier concentration at low temperature. As shown in Fig. 1(b), the epitaxial structure has three conduction layers such as GaN/sapphire interface layer,[32–35] n^+-GaN layer, and the GaN bulk layer. Generally, the GaN/sapphire interface and the n^+-GaN are degenerate layers, which add additional parallel conducting channels and affect the conduction of GaN bulk layer at all temperatures.[32–35] As reported in previous works, the donor band would merge with the conduction band and produce zero activation energy. This zero-activation energy is achieved when the density of carrier is higher than 6×10^{18} cm^{-3}. Due to similar conduction behavior, we simplified these two degenerate layers as one single layer and extract the electron concentration and mobility of bulk layer. These are calculated with the help of a bilayers conduction model as reported by Look and Molnar.[8] In this model, the total sheet conductance σ_s is considered to be the sum of the sheet conductance in all conductance channels:

$$\mu_1 = \frac{\mu_H^2 n_H - \mu_{LT}^2 n_{s\text{-}LT}/d}{\mu_H n_H - \mu_{LT} n_{s\text{-}LT}/d}, \tag{1}$$

$$n_1 = \frac{(\mu_H n_H - \mu_{LT} n_{s\text{-}LT}/d)^2}{\mu_H^2 n_H - \mu_{LT}^2 n_{s\text{-}LT}/d}, \tag{2}$$

where μ_1 and n_1 are the mobility and electron concentration of the bulk layer, which can be extracted from μ_H and n_H (the mobility and electron concentration of measurement by Hall), $n_{S\text{-}LT}$ and μ_{LT} are the sheet carrier concentration and mobility of the degenerate layer at low temperature and can be obtained from an open circle in Fig. 3.

Generally, the variation of background concentration can be affected by donor impurity (Si, O), point defect (V_N, C_N, C_{Ga}, *etc.*), and dislocations (change insignificantly here). The SIMS measurements are shown in Fig. 1(c), where we can see that the Si concentration is close to the detector limitation, and

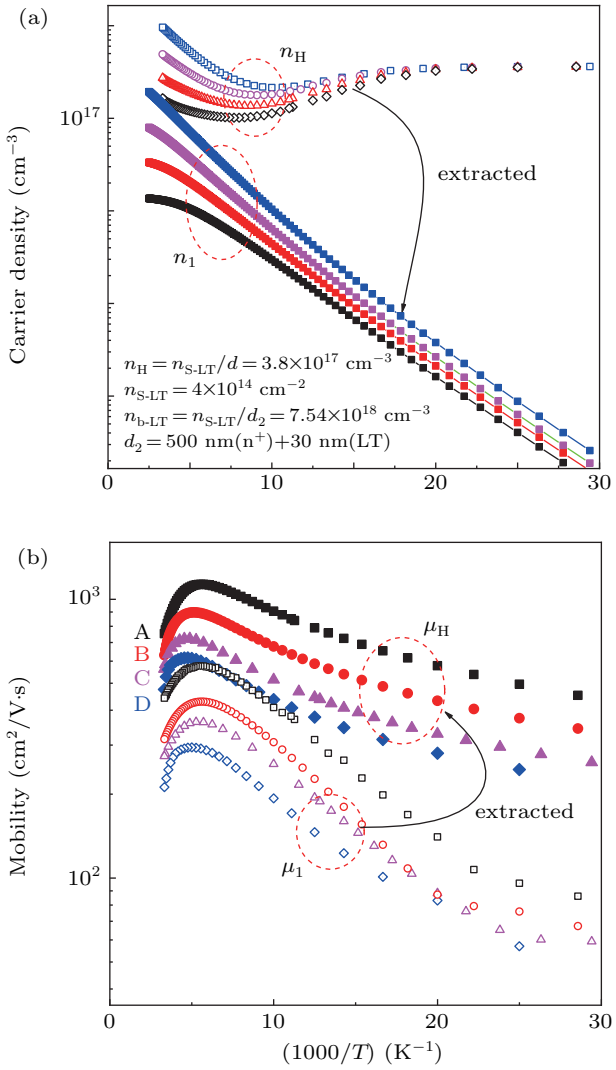


Fig. 3. The measured and extracted temperature-dependent electron concentration (a) and mobility (b) of the GaN bulk material based on the two-layer Hall model. n_H and n_1 are measured and extracted data, bulk carrier $n_{b\text{-}LT}$ is the bulk carrier concentration of degenerate layer at low temperatures.

oxygen is kept at approximately 5×10^{16} cm^{-3} for all samples. Both the Si and O concentrations have no obvious variation with the reactor pressure. On the other hand, the variation in concentration of carbon has a direct relation with the reactor pressure. Therefore, we suggest that the most possible source for the background carrier is a point defect. PL measurement has been employed (Fig. 4(a)) to confirm the carbon acceptor levels, with BL, YL, and BE peaks at around 2.8, 2.2, and 3.4 eV, respectively. Comparative results of the intensity ratio of BL and YL with the BE are shown in Fig. 4(b). From Fig. 4(b), it can be inferred that the intensity of YL increases with carbon doping, and the BL is enhanced when the carbon exceeded 1×10^{17} cm^{-3}. This result confirms that the concentration of C_N in GaN layer increases along with the increase in carbon concentration. However, as reported in previous works, only approximately 1% of the incorporated carbon atoms can be transformed into the active C_N acceptor (approximately 1×10^{16} cm^{-3} in our experiment).[31] This concentration is not enough to pin the Fermi level at around C_N acceptor, resulting in an n-type conduction. So, there might be other reasons which can decrease the carrier concentration.

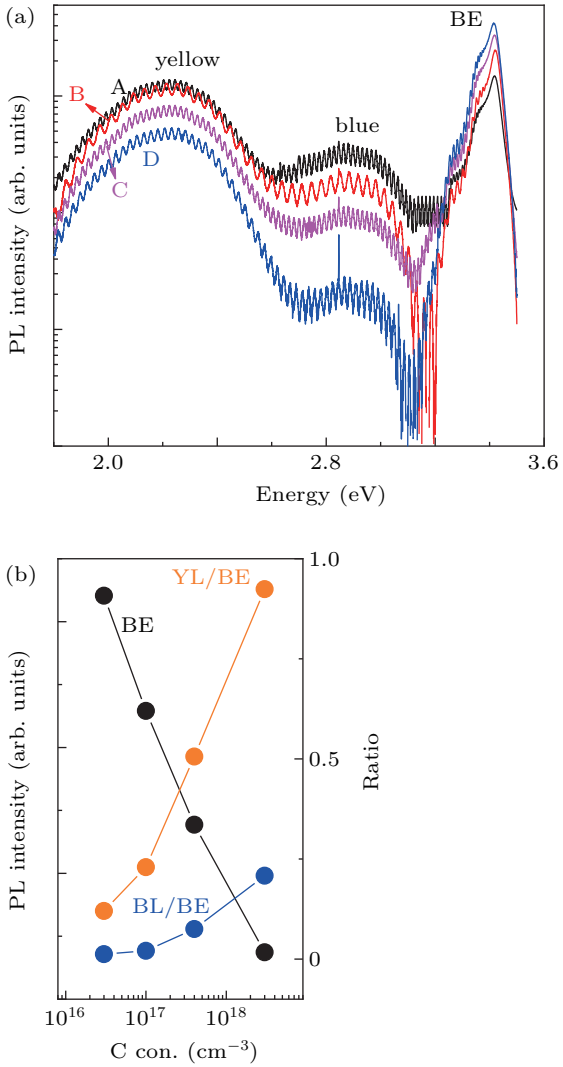


Fig. 4. (a) Room-temperature photoluminescence spectrum. (b) The ratio of intensity of blue luminescence and yellow luminescence with the band edge luminescence.

To evaluate the contribution of possible impurities (O, C, V_N, *etc.*) on the conduction of GaN, we fitted the temperature-dependent carrier concentration with the following ionization theory.[27,36] Here, we considered the carrier concentration as the sum of all impurities, which are ionized simultaneously *versus* temperature, as shown in Fig. 5

$$n - N_{\text{comp}} = \sum_{i=1}^{M} \frac{N_{\text{Di}}}{1 + \left(\frac{g_i n}{N_C}\right) \exp\left(\frac{\Delta E_{\text{Di}}}{kT}\right)} - \sum_{i=1}^{N} \frac{N_{\text{Ai}}}{1 + \left(\frac{g_i n}{N_V}\right) \exp\left(\frac{\Delta E_{\text{Ai}}}{kT}\right)}.$$

In this equation, n is the electron concentration, N_{comp} is the hole concentration of background compensating impurities, M and N are the numbers of donors and acceptor, ΔE_{Di} (ΔE_{Ai}) and N_{Di} (N_{Ai}) are the activation energy and concentration of

the donor (acceptor), g_i is the degeneracy factor of the electronic states in the band gap. g_i is considered to be 2 and 4 for donor and acceptor, respectively. The expressions

$$N_{\mathrm{C}} = \frac{2\left(2\pi m_{\mathrm{n}}^{*} kT\right)^{3/2}}{h^3} \quad \text{and} \quad N_{\mathrm{V}} = \frac{2\left(2\pi m_{\mathrm{p}}^{*} kT\right)^{3/2}}{h^3}$$

are the effective state density of conduction and valence band. The effective electron mass of $0.2m_0$ (m_0 is the free electron mass).

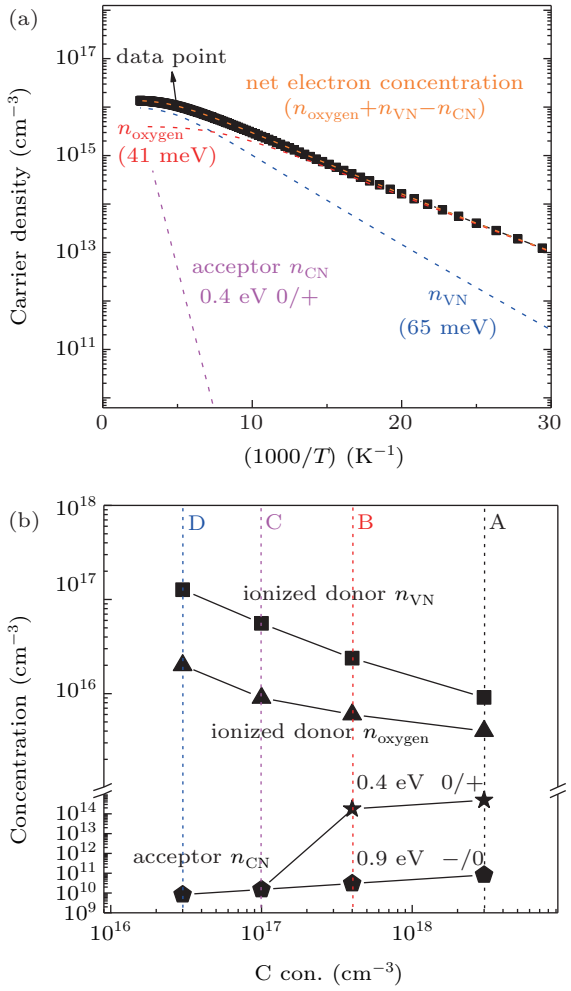


Fig. 5. (a) Typical numerical fitting of the temperature-dependent carrier concentration of sample A, short dash lines are fitted data (orange: total ionized net electron concentration, red: ionized oxygen concentration, pink: ionized C_N acceptor concentration, blue: ionized nitrogen vacancy concentration), the black square is the experimental data. (b) The extracted parameters of samples at different carbon dopings.

As shown in Fig. 5(a), the Hall data of sample A is well fitted with three kinds of impurities based on the previous discussion. The oxygen impurity (O_N)[3] with a relatively smaller activation energy of 41 meV (much greater than that of Si) is obtained from the Arrhenius equation (Fig. 5(a)) which dominates the carrier at low temperature, and finally, it is saturated at room temperature (red dotted line in Fig. 5(a)). Therefore, nitrogen–vacancy (V_N)[8] with a higher activation energy of 65 meV is obtained from the Arrhenius equation which plays a key role at room temperature. The C_N acceptor with a 0.4-eV level is also considered. However, the ionized C_N concentration is lower by a few orders of magnitude. This result is also consistent with the already reported work that the C_N cannot produce p-type conductivity at room temperature. From Fig. 5(b), we can observe that both the nitrogen–vacancy and ionized oxygen decrease with the increasing of carbon concentration. However, the concentration of oxygen does not change along with the concentration of carbon doping, as shown in the SIMS measurement. This may be related to the formation of C_NO_N[24] complex which is a deep trap (0.75 eV above the valence band) and also contributes to the YL band.

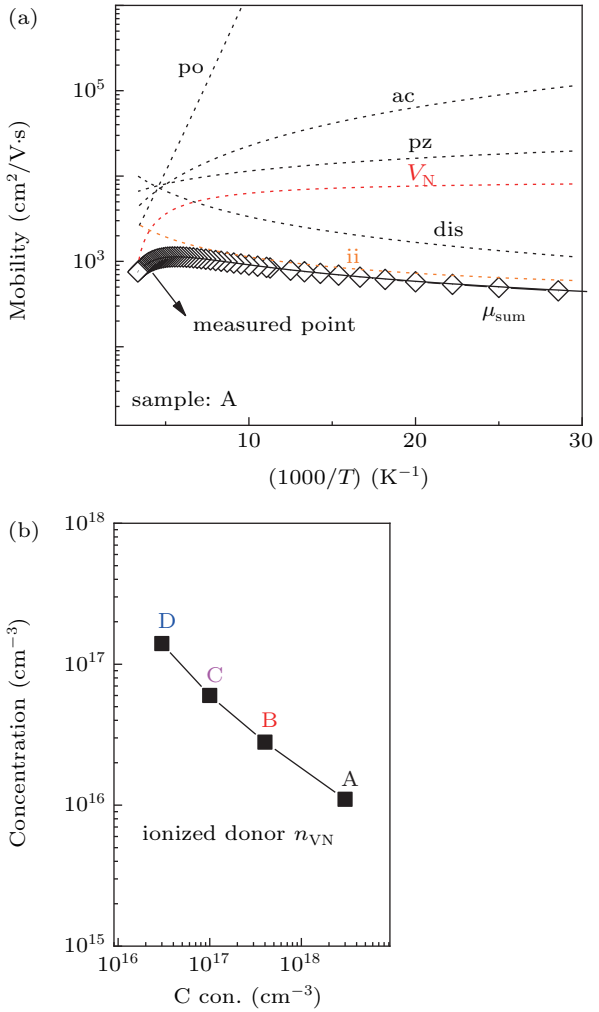


Fig. 6. Typically mobility fitting curves of sample A using Matthiesen's rule (a), "ii" represents the ionized impurity scattering, "dis" represents the dislocation scattering, "V_N" represents the nitrogen–vacancy scattering, "pz" represents the piezoelectric potential scattering, "ac" represents the acoustic deformation potential scattering, "po" represents the polar optical phonon scattering. The extracted nitrogen vacancy values *versus* the carbon concentration (b).

The contribution of ionized impurities to the conduction can also be obtained from the temperature-dependent mobility curves. Generally, the mobility can be analyzed from Matthiesen's rule ($1/\mu = \sum \mu i$), assuming the scattering events are independent of each other. In our fitting, the key scattering items are comprised of ionized impurity scattering with the donor and acceptor concentration which are de-

rived from carrier concentration fitting, polar optical phonon scattering (po), acoustic deformation potential scattering (ac), piezoelectric potential scattering (pz), and dislocation scattering (dis) as reported in previous literature.[8,37] The concentration of V_N is chosen as the only variable for the numerical fitting of mobility (Fig. 6) with its scattering contribution which is described[35]

$$\mu_{V_N} = \frac{9}{16\sqrt{3}} \frac{h^4 e}{m^{*5/2} N_{V_N}} \frac{1}{U_0^2 a^6} (k_B T)^{-1/2}.$$

Based on a simple square-well scattering potential with well depth $U_0 = 2$ eV and width $a = c = 5.1$ Å, the fitting results are shown in Fig. 6. Analysis of Fig. 6 demonstrates that the nitrogen–vacancy decreases with the increase in carbon concentration. This result is consistent with the carrier fitting data as shown in Fig. 5(b) and also summarized in Table 1.

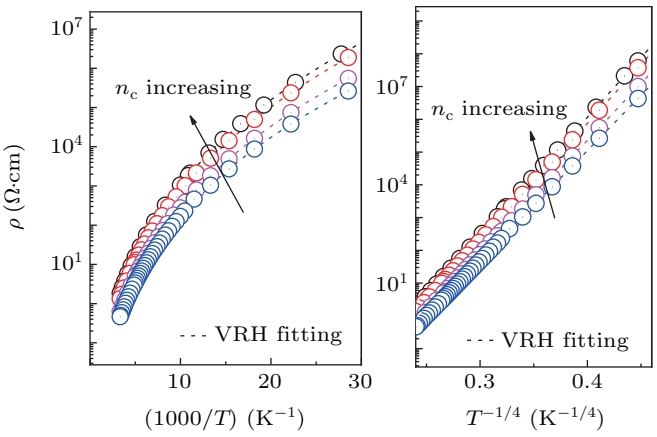


Fig. 7. Temperature dependence of (a) resistivity calculated by extracted n and μ,variable range hopping fitting formula (5) was used, (b) $T^{-1/4}$ dependence of resistivity. The hollow circle is data point, short dashes are the fitting data.

When the ionization of impurities is suppressed and the carrier is frozen to the donor level, then the donor energy levels contribute to the hopping conduction mode in GaN at the low-temperature region. So, the conduction cannot be determined by the conduction band but the shallow donor such as O_N and V_N. Therefore, the donor density can be extracted from the hopping conduction fitting. Hopping conduction transportation is commonly found at low temperatures which show a clear non-zero temperature dependence law of $T^{-1/4}$.[9,38] The donor density N_D concentration is calculated from the variable range hopping fitting:

$$\rho_{vr} = C_{vr} e^{(T_0/T)^{1/4}} = \frac{1}{ne\mu},$$

where C_{vr} is a constant, $T_0 \approx 21.3/kg(\varepsilon)a_d^3$.

Variable $g(\varepsilon)$ is the density of states at the Fermi level. Since the number of empty states in the donor band is equal to the concentration of acceptor, we can approximate $g(\varepsilon) \approx N_A/\varepsilon$, $\varepsilon \approx 0.99e^2 N_D^{1/3}/4\pi kR$, the concentration of donor N_D and acceptor N_A are all obtained from the fitting parameters of carrier concentration above, $a_d \approx 10$ Å is the extent of the defect wave function, the nearest neighbour $R = (3/4\pi N_D)^{1/3}$. The resistivity of four samples is plotted *versus* $T^{-1/4}$ in Fig. 7(a) with good linearity, indicating the variable range hopping conduction mechanism at low temperature. The obtained N_D for all samples is summarized in Table 1, Comparative results and discussion of the data of Table 1 lead us to conclude that these results have a good agreement with that of Hall data fitting.

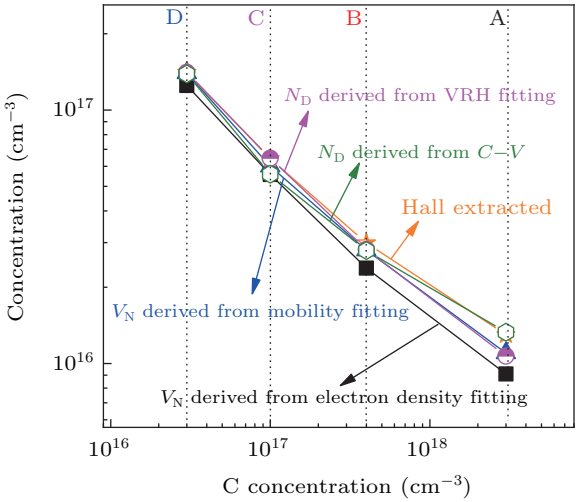


Fig. 8. Comparison of V_N and carrier concentration extracted from the experimental and numerical fitting at room temperature.

The nitrogen–vacancy concentration is calculated from different methods as well as the background net carrier concentration *versus* the carbon concentration, as shown in Fig. 8. It is found that the background carrier density and V_N concentration are comparable, and show a similar decreasing trend along with the increase in carbon concentration. Besides, the ionized C_N is 1–2 order of magnitude lower than that of donor impurity in the case of samples A and B with high carbon concentration and above 6 order of magnitude lower in samples C and D (Fig. 5(b)). The reason behind this is the high ionization energy of C_N. Therefore, it is proposed that the reduction of carrier concentration at room temperature is because of acceptor compensation but the decreasing of V_N along with carbon doping. It is worth noting that the decreasing of carbon concentration is nearly one order of magnitude larger than that of the variation of background carrier density. This may be due to the nitrogen sites of the GaN lattice, which can be filled by nitrogen (Ga–N bond), empty (V_N), and occupied by oxygen (O_N). The reduction in V_N is obtained when the carbon atoms fill the empty nitrogen sites and consequently reduce the carrier density. However, the carbon atoms can also substitute the nitrogen atom (Ga–C bond) and/or form C_NO_N complex. So, only part of the carbon atoms can reduce the background concentration. For the sample at a higher concentration of carbon doping, the difference between the V_N and O_N concentrations (sample A of Fig. 5(b)) became smaller and enhance the

contribution of O_N to the conduction. Finally, this causes the undesired deviation of N_D which is extracted from different methods (as shown in Fig. 8 and Table 1).

4. Summary and conclusions

In summary, the mechanism of high resistive GaN by applying carbon doping has been studied to investigate the impact of carbon concentration on the background carrier conduction. As expected, the incorporation of carbon atom has effectively suppressed the n-type background carrier concentration. By fitting the carrier concentration and mobility curves, it is found that the n-type conduction of GaN is mainly originated from the nitrogen–vacancy (V_N) at room temperature. The Fermi level pinning effect at around C_N acceptor can be excluded for the reduction of background carrier concentration. The PL characterizations showed that carbon is a preferable dopant and occupy the nitrogen site, and form a deep C_N acceptor in the resulted GaN. Later, we found that an extremely low hole concentration can be ionized at room temperature, which is insufficient to compensate the background carriers. So, it is concluded that the carrier suppression is because of the substitution of V_N by carbon doping and not by the acceptor trap.

References

[1] Niraj M S, Yiming L, Tetsuya S and Seiji S 2019 *IEEE Trans. Electron Dev.* **66** 2901719

[2] Gupta C, Lund C, Chan S H, Anchal A, Liu J, Enatsu Y, Keller S and Mishra U K 2017 *IEEE Electron Dev. Lett.* **38** 353

[3] Meyer B K, Volm D, Graber A, Alt H C, Detchprohm T, Amano A and Akasaki I 1995 *Solid-State Commun.* **95** 597

[4] Götz W and Johnson N, Chen M C, Liu H, Kuo C and Imler W 1996 *Appl. Phys. Lett.* **68** 3144

[5] Ganchenkova M G and Nieminen R M 2006 *Phys. Rev. Lett.* **96** 196402

[6] Perlin P, Suski T, Teisseyre H, Leszczynski M, Grzegory I, Jun J, Porowski S, Boguskawski P, Bernholc J, Chervin J C, Polian A and Moustakas T D 1995 *Phys. Rev. Lett.* **75** 296

[7] Mattila T and Nieminen R M 1997 *Phys. Rev. B* **55** 9571

[8] Look D C, Farlow G C, Drevinsky P J, Bliss D F and Sizelove J R 2003 *Appl. Phys. Lett.* **83** 3525

[9] Look D C and Reynolds D C 1996 *J. Appl. Phys.* **80** 2960

[10] Koleske D D, Wickenden A E and Henry R L 2002 *J. Crystal Growth* **242** 55

[11] Polyakov A Y, Smirnov N B, Govorkov A V, Vdovin V I, Markov A V, A Shlensky A, Prebble E, Hanser D, Zavada J M and Pearton S J 2007 *J. Vac. Sci. Technol. B* **25** 436

[12] Iwinska M, Piotrzkowski R, Litwin-Staszewska E, Yu Ivanov V, Teisseyre H, Amilusik M, Lucznik B, Fijalkowski M, Sochacki T, Takekawa N, Murakami H and Bockowski M 2017 *J. Crystal Growth* **475** 121

[13] Li X, Bergsten J, Nilsson D, Danielsson Ö, Pedersen H, Rorsman N, Janzén E and Forsberg U 2015 *Appl. Phys. Lett.* **107** 262105

[14] Ni Y Q, Li L, He L, Que T T, Liu Z X, He L, Wu Z S and Liu Y 2018 *Superlattices and Microstructures* **120** 720

[15] Ni Y Q, Zhou D Q, Chen Z J, Zheng Y, He Z Y, Yang F, Yao Y, Zhou G L, Shen Z, Zhong J, Wu Z S, Zhang B J and Liu Y 2015 *Semicond. Sci. Technol.* **30** 105037

[16] Lundin W V, Zavarin E E, Brunkov P N, Yagovkina M A, Sakharov A V, Sinitsyn M A, Ber B Y, Kazantsev D Y and Tsatsulnikov A F 2016 *Technical Physics Letters* **42** 539

[17] Kato S, Satoh Y, Sasaki H, Masayuki I and Yoshida S 2007 *J. Crystal Growth* **298** 831

[18] Hady Y, Thorsten Z, Gerrit L, Hannes B, Dirk F, Martin E, Michael H, Holger K and Andrei V 2018 *IEEE Trans. Electron Dev.* **65** 2850066

[19] Xu Y, Li Z Q, Yang X L, Shi L, Zhang P, Cao X Z, Nie J F, Wu S H, Zhang J, Feng Y X, Zhang Y, Wang X Q, Ge W K, Xu K and Shen B 2019 *Jpn. J. Appl. Phys.* **58** 090901

[20] Villamin M E, Kondo T and Iwata N 2021 *Jpn. J. Appl. Phys.* **60** SBBD17)

[21] Kozawa T, Kachi T, Kano H and Nagase H 1995 *J. Appl. Phys.* **77** 4389

[22] Kisielowski C, Kruger J, Ruvimov S, Suski T, Ager J W, Jones E, Liliental-Weber Z, Rubin M, Weber E R, Bremser M D and Davis R F 1996 *Phys. Rev. B* **54** 17745

[23] Wu S, Yang X L, Zhang H S, Shi L, Zhang Q, Shang Q Y, Qi Z M, Xu Y, Zhang J, Tang N, Wang X Q, Ge W K, Xu K and Shen B 2018 *Phys. Rev. Lett.* **121** 145505

[24] Reshchikov M A, Vorobiov M, Demchenko D O, ÖzgürÜ, Morkoç H, Lesnik A, Hoffmann M P, Hörich F, Dadgar A and Strittmatter A 2018 *Phys. Rev. B* **98** 125207

[25] Lyons J L, Janotti A and Van C G de Walle 2014 *Phys. Rev. B* **89** 035204

[26] Seager C H, Wright A F, Yu J and Götz W 2002 *J. Appl. Phys.* **92** 6553

[27] Jain S C, Willander M, Narayan J and Overstraeten R V 2000 *J. Appl. Phys.* **87** 965

[28] Narita T, Tomita K, Kataoka K, Tokuda Y, Kogiso T, Hikaru Y, Ikarashi N, Iwata K, Nagao M, Sawada N, Horita M, Suda J and Kachi T 2019 *Jpn. J. Appl. Phys.* **58** SIIA16

[29] Chini A, Meneghesso G, Meneghini M, FantinF i, Verzellesi G, Patti A and Iucolano F 2016 *IEEE Trans. Electron Dev.* **63** 3473

[30] Remesh N, Mohan N, Raghavan S, Muralidharan R and Nath D N 2020 *Trans. Electron Dev.* **67** 2311

[31] Honda U, Yamada Y, Tokuda Y and Shiojima K 2012 *Jpn. J. Appl. Phys.* **51** 04DF04

[32] Götz W, Walker J, Romano L T, Johnson N M and Molnar R J 1996 *MRS Proc.* **10** 1557

[33] Xu X L, Beling C D, Fung S, Zhao Y W, Sun N F, Sun T N, Zhang Q L, Zhan H H, Sun B Q, Wang J N, Ge W K and Wong P C 1999 *Appl. Phys. Lett.* **76** 125686

[34] Huang Y, Chen X D, Fung S, Beling C D, Ling C C, Wei Z F, Xu S J and Zhi C Y 2000 *J. Appl. Phys.* **96** 1763235

[35] Look D C and Molnar R J 1997 *Appl. Phys. Lett.* **70** 3377

[36] Götz W, Chen C, Liu H, Kuo C and Imler W 1996 *Appl. Phys. Lett.* **68** 3144

[37] Zhu Q S and Sawaki N 2000 *Appl. Phys. Lett.* **76** 126106

[38] Robert M H 1971 *Philosophical Magazine* **24** 1307